JMEPEG
https://doi.org/10.1007/s11665-024-09287-9

1059-9495/$19.00

ORIGINAL RESEARCH ARTICLE

Qualification of Austenitic Stainless Steels for the Development of Load-Sensitive Material Sensors

René Gansel, Markus Quanz, Armin Lohrengel, Hans Jürgen Maier, and Sebastian Barton

Submitted: 14 July 2023 / Revised: 2 November 2023 / Accepted: 2 February 2024

To detect mechanical overloads on the component directly in operation, a metastable material can be used as a load-sensitive sensor when combined with an eddy current testing system. In order to find a suitable metastable sensor material that exhibits microstructural changes at an early stage before fatigue failure, quasi-static tensile tests and cyclic rotating bending tests were carried out with the austenitic stainless steels 1.4301 (2 batches), 1.4305, 1.4541 and 1.4550. For the detection of microstructural changes, electromagnetic testing was used in-situ in the tensile test and ex-situ between the rotating bending test after a pre-defined number of cycles. The investigated materials 1.4301 batch2 and 1.4550 showed the largest signal changes and the lowest austenite stability both in the tensile test and under cyclic bending load. Due to the better mechanical properties, 1.4301 batch2 should be preferred. The order of the austenitic stainless steels tested was similar in terms of transformation behavior in both tests. Thus, the tensile test combined with in-situ electromagnetic testing appears to have potential as a suitable benchmark test for austenite stability. With regard to the cyclic bending stress, an overload of the specimens could be detected for the materials 1.4301 batch2, 1.4305, 1.4541 and for the 1.4550 on the basis of a significant amplitude change. At low bending stresses, uncritical for structural integrity, no increase in amplitude was measured. The results have shown that an early detection of overloads is possible with several materials, however, the potential for detecting overloads varies between materials and also between individual batches. In addition, it has been observed that as the bending stress increases, the gradient of the change in amplitude over the number of cycles increases as well. Thus, with a known number of cycles, it could be possible to classify the previous load spectrum based on the difference in amplitude between two measurements.

Keywords austenitic stainless steel, electromagnetic testing, fatigue state, material sensor, non-destructive testing, overload monitoring

1. Introduction

The monitoring and analysis of technical systems and components is becoming increasingly important to ensure high availability and safety. In this context, it is crucial to obtain precise information about the condition of the components directly during operation. Continuous monitoring of loads allows deviations from the normative load curve to be detected at an early stage so that appropriate countermeasures can be taken. Early detection of damage-relevant loads is an important factor as it enables proactive maintenance, and thus prevents unexpected downtimes. In addition, the service life of entire plants can be extended through an accurate service life estimation of the components, thus increasing economic efficiency.

René Gansel, Hans Jürgen Maier, and **Sebastian Barton**, Institut für Werkstoffkunde (Materials Science), Leibniz Universität Hannover, 30823 Garbsen, Germany; and **Markus Quanz** and **Armin Lohrengel**, Institut für Maschinenwesen (Mechanical Engineering), TU Clausthal, 38678 Clausthal-Zellerfeld, Germany. Contact e-mail: gansel@iw.uni-hannover.de.

As part of the Priority Program 2305 (Sensor-Integrated Machine Elements pave the way for Widespread Digitization), the present projects tries to implement an energy-autonomous, non-destructive in-situ condition monitoring on the demonstrator component splined shaft by combining material sensors and eddy current sensors, see [1] for detailed information. An exemplary concept for load monitoring of a splined shaft consisting of material and eddy current sensors and an evaluation unit is shown in Fig. 1. The material sensor will be produced locally by means of laser heat treatment in a martensitic surface layer on an austenitic stainless steel base material. The permanently applied eddy current sensors should be compact and energy-efficient, but still have a high sensitivity. The evaluation unit will consist of a microcontroller and peripherals and will ensure wireless data transmission. The necessary energy will be generated by means of energy harvesting.

The principle of the material sensor is based on a structural transformation of paramagnetic austenite to ferromagnetic martensite when a certain load threshold value is exceeded. Due to the lower strength, only the material sensor is subject to microstructural changes. These magnetic changes can be detected using electromagnetic testing technology. Upon mechanical loading, the formation of martensite proceeds stepwise and irreversibly as a function of the applied load amplitude and number of cycles. The change in martensite content can be related to the load history. Furthermore, cyclic electromagnetic tests and subsequent analysis of the signal changes can be used to detect possible damage to the

Published online: 11 March 2024

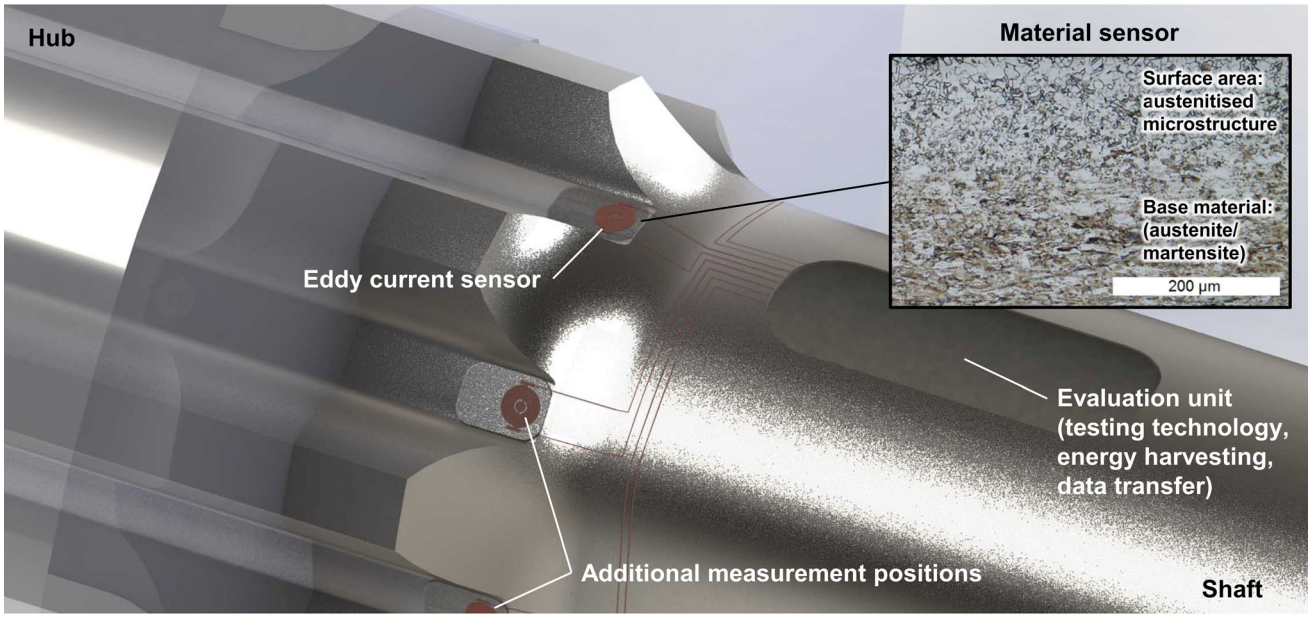

Fig. 1 Exemplary concept consisting of material and eddy current sensors and an evaluation unit for load monitoring of a splined shaft

components at an early stage and estimate the remaining service life.

Currently, there is no way to order the austenite stability desired for the material sensor in semi-finished products in a controlled manner. Therefore, various austenitic stainless steels with different contents of chemical elements such as C, Cr and Ni were investigated in terms of their potential for the mechanically-induced austenite to martensite formation. Despite the existing literature on the formation of martensite in austenitic stainless steels, actual testing is required as a theoretical determination of metastability using parameters such as martensite start (M_s) temperature, martensite deformation (M_d) temperature and stacking fault energy (γ_{SF}) are subject to significant variations, depending on the formula chosen [2, 3]. In addition, when comparing two batches of the same alloy, the potential for martensite formation can be significantly different, as the individual chemical elements are only required to be within a certain range according to the standard [2-4]. The aim of the present study was to determine an alloy or rather a chemical composition that allows to detect critical loads as early as possible before fatigue failure, based on the structural change. Under the normal operating conditions, however, the structural change should not take place. The metastability of the alloys 1.4301 batch1 and batch2 (AISI 304), 1.4305 (AISI 303), 1.4541 (AISI 321) and 1.4550 (AISI 347) was evaluated by quasi-static tensile tests and cyclic rotating bending tests. Electromagnetic testing signals provided the main data for the evaluation of the metastability. Tensile tests were carried out to determine the yield strength for the cyclic bending tests and to detect in situ microstructural changes, especially the necessary plastic strain, under the same test conditions for each material. The cyclic bending tests were chosen to investigate a type of stress state that also occurs in the loading of splined shafts. The objective of the tests was to find prerequisites for a material sensor that would show initial microstructural changes under cyclic stresses well below the critical load limit. Therefore, the following aspects need to be investigated in the literature as well as in practical tests:

- What are the factors that have an influence on the austenite stability?
- How can the austenite stability be determined or compared?
- Which alloy exhibits low austenite stability and can be used for the material sensor?
- Which non-destructive testing methods are suitable to detect in-situ structural changes or rather to evaluate the fatigue state?

2. State of the Art

2.1 Martensite Formation

With regard to the material sensor, the potential of austenitic stainless steels for martensite formation is essential. Specifically, the overloads have to be detected based on microstructural changes occurring in areas that do not have a critical influence on the structural integrity. The metastability of austenitic stainless steels depends on a wide variety of factors. Basically, according to Olson and Cohen, martensite can be thermally induced, stress-induced or strain-induced. Strain-induced martensite formation occurs when there is sufficient strain applied in the temperature range between the M_d and $M_{S,\sigma}$ temperatures. In this case, the nucleation sites are generated by the plastic deformation. Above the M_d temperature, plastic deformation becomes excessive before martensite formation occurs. Between the $M_{S,\sigma}$- and M_S-temperatures, stress-induced martensite occurs at nucleation sites where thermally-induced martensite formation could also be initiated. In this range, martensite formation can already occur under elastic deformation, provided that the combination of chemical driving force and mechanical stress is sufficiently high. Below M_S, thermally-induced martensite formation is possible [5]. The austenite stability mostly depends on the chemical composition, the microstructure, the previous load history, the load amplitude

and the operating temperature. For theoretical estimation of metastability, the M_S and the M_{d30} temperature are often used in the literature. The M_{d30} temperature indicates the temperature at which 50% martensite content should be present after 30% deformation. In addition, the stacking fault energy (γ_{SF}) can also be used to estimate metastability. With regard to the three parameters, it should be noted that there are a large number of different formulas for each parameter, which differ mainly in the weighting of the respective alloying elements. In the present study, the formulas most frequently used in the literature were employed for the estimation of the respective parameter, i.e.:

$$M_{d30}\text{ according to Angel[6]}(^\circ\text{C}) = 413 - 462(\text{C}+\text{N}) - 9.2\text{Si} - 8.1\text{Mn} - 13.7\text{Cr} - 9.5\text{Ni} - 18.5\text{Mo} \quad \text{(Eq 1)}$$

$$M_S\text{ according to Pickering [7]}(^\circ\text{C}) = 502 - 810\text{C} - 1230\text{N} - 13\text{Mn} - 30\text{Ni} - 12\text{Cr} - 54\text{Cu} - 46\text{Mo} \quad \text{(Eq 2)}$$

$$\gamma_{SF}\text{ according to Pickering [8]}\left(\text{mJ/m}^2\right) = 25.7 + 2\text{Ni} + 410\text{C} - 0.9\text{Cr} - 77\text{N} - 13\text{Si} - 1.2\text{Mn} \quad \text{(Eq 3)}$$

where the alloying element contents must be used here in mass percent. In summary, the alloying elements C, N, Cr and Ni have a pronounced influence on the three parameters considered. With regard to γ_{SF}, the temperature dependence must also be taken into account [9]. In principle, martensite formation can occur from γ-austenite (fcc) via ε-martensite (hcp) into α'-martensite (bcc) or directly into α'-martensite. At high stacking fault energies, dislocation slip is the primary mechanism of α'-martensite formation. At lower γ_{SF}, formation via ε-martensite and deformation twinning is the primary mechanism [5, 9-11]. Schumann reports a γ_{SF} of 20 mJ/m^2 as a reference value for FeCrNi systems; below this stacking fault energy, 100% strain-induced α'-martensite should occur under favorable thermodynamic conditions [12].

2.2 Summary of Findings from the Literature Relating to a Load Sensitive Material

It can be stated that for known loads it is possible to predict the fatigue state from the martensite content [2, 13]. However, this is more difficult with changing or rather unknown loads [2]. In addition, ambient temperature [2, 3, 14], loading frequency (strain rate) and resulting specimen temperature [15-19] as well as grain size have an influence on the formation of martensite [20, 21], although the latter is not clearly understood in the literature. Non-destructive testing has been used to compare the potential for martensite formation in different materials and a significant batch effect has been demonstrated for, e.g., 1.4550 [4].

Regarding the non-destructive evaluation of the fatigue state, it can be summarized that structural change can be detected qualitatively using eddy current coils (e.g., pancake coils [22-24]) and impedance evaluation [3, 18, 25, 26]. The Villari effect was found to be a significant disturbance in the eddy current tests [27-29]. For quantitative determination of the magnetic content in the microstructure, a Feritscope or SQUID measurements are typically used, with XRD measurements as a reference [28, 30]. Quantitative determination by metallography shows greater variation in comparison [28]. However, these quantitative methods are not suitable for permanent application to a component. Eddy current coils, on the other hand, can be used for permanent application, for instance permanently on fatigue specimen [25] or on bolts [24].

The literature also shows that for the materials used (mostly 1.4301, 1.4541 and 1.4550) small changes in Cr or Ni content have a significant effect on austenite stability and hence on the potential for martensite formation above a certain load limit [3, 4, 31]. Currently, there is no possibility to order austenite stability for semi-finished products in a controlled and reproducible way. The theoretical estimation of the austenite stability, e.g., by means of the M_{d30} temperature, is not reliable, which means that practical benchmark tests to evaluate the austenite stability are indispensable [2, 3]. Tensile tests [27, 28, 32, 33] have shown that the austenitic stainless steels investigated require a critical deformation, starting from 5 to 10% or more plastic deformation, to produce the first structural changes, making early detection of overload more difficult [34]. Yet, there is a lack of information about the transformation behavior of components consisting of austenitic stainless steel under cyclic loading. In addition, changing ambient temperatures present a challenge in terms of martensite formation and interpretation of the fatigue state, as the same load can lead to martensite formation at room temperature, less or no martensite formation can occur at higher temperatures [3, 34]. The sensitivity of the NDT technique should also be mentioned as an important aspect in the evaluation of the fatigue state, since despite a high austenite stability of the material, small structural changes can still be detected with high sensitivity and included in the evaluation [14].

3. Materials and Methods

3.1 Materials

The materials investigated in the present study were austenitic metastable stainless steels, whose chemical composition are given in Table 1. The material was supplied as drawn bar stock of various diameters in the solution-annealed condition.

The calculated M_{d30} and M_S temperatures as well as γ_{SF} values were intended to serve as a priori estimate of metastability and represent estimated values only, since aspects such as grain size, type of deformation and previous thermal/mechanical loads as well as, in the case of the stacking fault energy, the prevailing temperature are not taken into account here. The aim was to find a stainless steel that already exhibits initial microstructural changes at stresses in the yield strength range. In theory, this requires positive M_{d30} and high M_S temperatures. A low stacking fault energy favors the formation of planar lattice defects, such as stacking faults, deformation twins or ε-martensite. These defects, in particular their intersections, can then serve as possible nucleation sites for the formation of α'-martensite. In terms of the three parameters, the 1.4301 batch2, 1.4541 and 1.4550 should have low austenite stability.

Table 1 Chemical composition of the investigated austenitic stainless steels (in wt.%) with balance Fe determined with spark spectroscopy.

Element	C	Si	Mn	Cr	Mo	Ni	Cu	N	M_{d30}	M_S	Y_{SF}
1.4301 batch1	0.036	0.36	1.82	18.29	0.18	7.93	0.39	0.110	− 2	− 164	25
1.4301 batch2	0.037	0.45	1.49	18.43	0.26	7.70	0.45	0.038	32	− 71	29
1.4305	0.066	0.26	2.05	17.69	0.12	8.01	0.80	0.079	7	− 170	41
1.4541	0.041	0.60	1.91	17.17	0.20	9.06	0.33	0.021	38	− 79	34
1.4550	0.050	0.48	1.01	17.51	0.33	9.17	0.39	0.029	31	− 95	39

The M_{d30} temperatures were calculated according to Angel [6] in °C, the M_S temperatures according to Pickering [7] in °C, and the stacking fault energy (γ_{SF}) in mJ/m^2 [8].

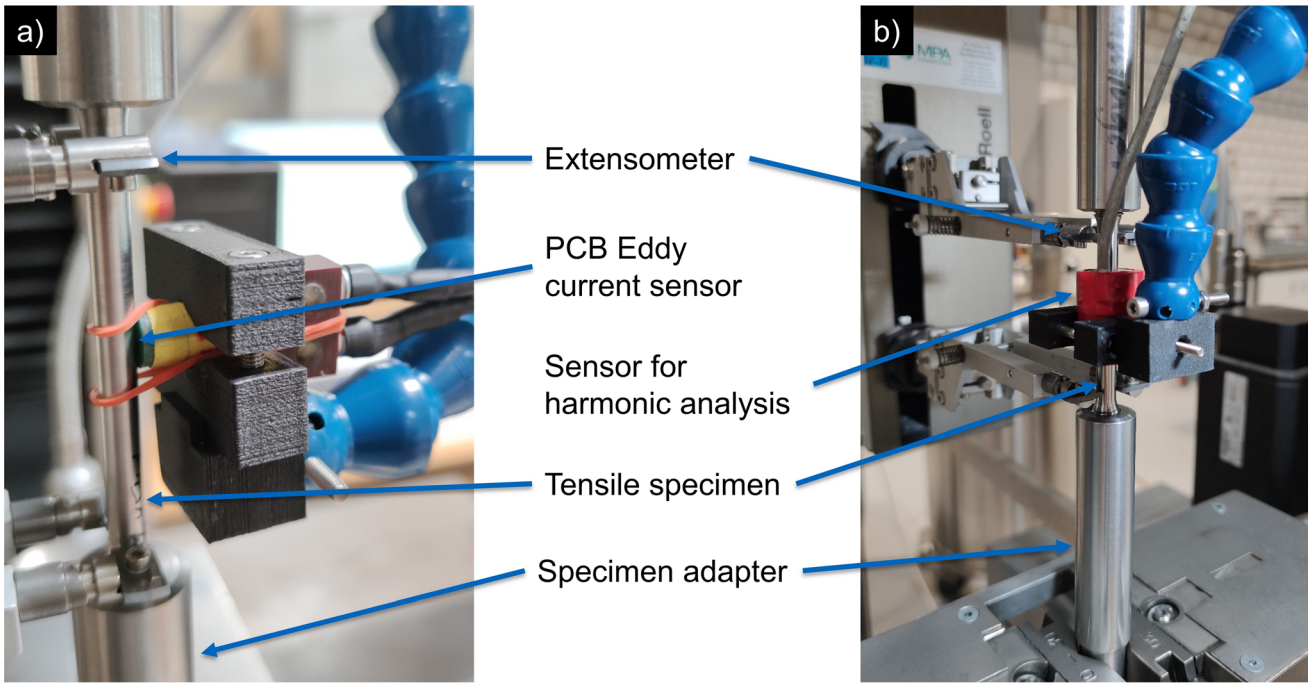

Fig. 2 Tensile test setup: (a) conventional eddy current testing (b) harmonic analysis

3.2 Detection of Microstructural Changes

Electromagnetic testing techniques was used both in- and ex-situ to detect changes in the microstructure directly during loading or after specific loading cycles. Both the conventional eddy current test and the magnetic inductive testing with analysis of the higher-harmonic signal components were carried out by a PK Computer with a measuring card and an in-house developed testing software. The sensors used in the following were also developed in-house. Conventional eddy current testing was used at a test frequency of 30 kHz in combination with a PCB (printed circuit board) eddy current probe (see Fig. 2a) consisting of measuring and exciter flat coils. The frequency of 30 kHz was determined in a parameter study using three calibration specimens with characterized martensite contents. At higher frequencies, the potential for distinguishing different martensite contents decreases. At lower frequencies, the sensitivity of the PCB sensor decreases. In the signal evaluation of the conventional eddy current test, the measurement signal is compared with the sinusoidal excitation signal. This way an amplitude and phase difference can be determined in the case of different eddy current formation. These two time-dependent parameters can be transformed into polar coordinates and then displayed in an impedance plane in the form of an operating point reflecting amplitude and phase [35, 36].

In addition, a circumferential sensor (see Fig. 2b), consisting of exciter, compensation and measuring coil, was used with a low excitation frequency of 400 Hz on the basis of a parameter study to enable the analysis of higher-harmonic signal components (also called harmonic analysis). With this method, when the field strength is high enough, detectable re-magnetization processes take place in ferromagnetic materials. These provide a magnetic hysteresis loop and at the same time a sinusoidal signal distorted with higher-harmonics. Whereas in austenitic, i.e., paramagnetic microstructures, the magnetic flux density is proportional to the magnetic field strength. The measurement signal can be divided into different frequency components using an FFT transformation. In particular, the amplitude of the 1st harmonic (excitation frequency) and the 3rd harmonic (in this case 1200 Hz) are essential parameters for

characterizing different microstructural components. From the 1st harmonic, electrical and magnetic properties can be derived. A 3rd harmonic, on the other hand, exists only if ferromagnetic material such as martensite is present. A pure austenitic component with low electrical conductivity and paramagnetic properties would therefore have a low 1st harmonic and no 3rd harmonic [37]. In principle, the amplitudes of the harmonics also increase with a higher content of magnetic material, e.g., martensite [32, 38].

Magnetic inductive testing with the analysis of higher-harmonic signal components was used because different investigations have demonstrated several times that a microstructure characterization is possible with this testing technique [29, 38-40]. This contrasts with conventional eddy current testing with PCB tactile sensors, which allow a reproducible and compact form due to the flat coil design and, at the same time, low-energy and low-data signal evaluation [35]. Flat coils would be one way to realize in-situ detection of component overloads on the splined shaft in accordance with the goal of the underlying research project (cf. Fig. 1). Another circumstance that argues against the use of magnetic inductive testing with harmonic analysis on a splined shaft is that a sufficiently large magnetic field must be generated to remagnetise the magnetic areas. This means that a high number of windings and/or a high current must be realized. The space available on the splined shaft is not sufficient for this. Nevertheless, magnetic inductive testing with harmonic analysis is also used in the following because of its sensitivity to structural changes.

In addition, XRD measurements using a Bruker Discover D8 X-ray diffractometer with a Co X-ray source were conducted. These data were used for the characterization of the microstructural changes after the end of the tests.

3.3 Tensile Tests

The transformation behavior of the solution-annealed materials were studied at room temperature in uniaxial tensile tests. The round specimens with a gauge diameter of 8 mm and a gauge length of 65 mm were tested in a Zwick-Roell Z100 (kN) universal tensile testing machine. The specimens had an M12 thread to connect them to adapters made of austenitic stainless steel. This minimized interference from the ferromagnetic clamping jaws of the tensile testing machine on the electromagnetic test signals.

The eddy current sensors were each placed in the center of the specimen and attached to the cross-head in order to move along with the strained specimen. Figure 2 shows the experimental setup used for the in-situ electromagnetic testing.

After each 5% elongation step, a 20 s hold phase was employed in the loaded and unloaded condition to reduce possible self-heating of the specimen and to allow accounting for the contribution of the Villari effect to the measurement signal. In addition, the influence of different strain rates ($2 * 10^{-1}\ s^{-1}$, $10^{-1}\ s^{-1}$, $10^{-2}\ s^{-1}$, $5 * 10^{-3}\ s^{-1}$) on the material behavior was investigated in preliminary tests using the signals from the harmonic analysis. Based on the preliminary tests and the literature [19, 27], a strain rate of $10^{-1}\ s^{-1}$ was selected for the subsequent tests. The purpose of the tensile tests was to determine the yield strength and to compare, under identical test conditions, the plastic deformation required to initiate martensite formation.

3.4 Rotating Bending Tests

A Zwick-Roell UBM 200 tC (rotating bending machine) was used to investigate martensite formation under cyclic loading, cf. Fig. 3. A sinusoidal alternating load is applied to round specimens, with the highest stress occurring in the specimen surface. The round specimens had a gauge diameter of 8 mm and a gauge length of 42 mm. The tests on the UBM can only be carried out under stress control. The parameters bending stress, loading frequency and number of load cycles can be varied. Based on the preliminary tests, a test frequency of 16.67 Hz was selected in order to minimize temperature increases in the specimen while allowing load cycles in the high-cycle fatigue (HCF) range.

The rotating bending tests were selected in order to investigate a type of stress state that also occurs in the loading of splined shafts. Furthermore, the stress amplitude for each material was specifically defined based on the yield strength. For each material, the stress amplitude was started at 50% of the yield strength. The stress strain diagram and the 0.2 pct offset yield strength σ_y determined from the tensile tests are shown in Fig. 4.

As can be seen, the deviations between the curves of a single material are negligible. However, when comparing alloys and batches, there are clear differences in tensile strength and yield strength. In comparison, the 1.4301 batch1 has the highest strength and the 1.4550 the lowest. The two batches of 1.4301 show a high difference of 110 MPa in the yield strength.

The magnetic inductive testing with the analysis of higher-harmonic signal components were performed with the circumferential sensor from Fig. 2b ex-situ after defined load cycles according to the following sequence: Initial condition, $5 * 10^4$, 10^5, $2 * 10^5$, $3 * 10^5$, $4 * 10^5$, $5 * 10^5$ cycles. For this purpose, the specimen was removed from the rotating bending test rig after the defined load cycles and tested in a suitable set-up. In the case of austenitic stainless steels, due to the formation of martensite and the resulting hardening, it can be assumed that if 500,000 cycles are achieved without failure, a fatigue strength of minimum $2 * 10^6$ cycles can be expected [41, 42].

The aim of the tests was to find a chemical composition that exhibits initial microstructural changes at stresses considerably below the load limit. The secondary objective was to detect possible component overload at an early stage by means of electromagnetic testing as well as to obtain information about the signal changes until fracture.

4. Results and Discussion

4.1 Tensile Tests

From the captured machine data and the electromagnetic test results, the change in amplitude as a function of plastic strain in the unloaded state was evaluated. Magnet inductive testing with analysis of higher-harmonic signal components by means of a circumferential sensor was carried out with the test frequency of 400 Hz.

In the following, the different microstructural changes as a function of plastic strain are compared on the basis of the electromagnetic signal changes and the results from the XRD measurements. In the testing signals of the magnetic inductive test and the eddy current test, the decreasing test volume with plastic deformation is not compensated, since all specimens

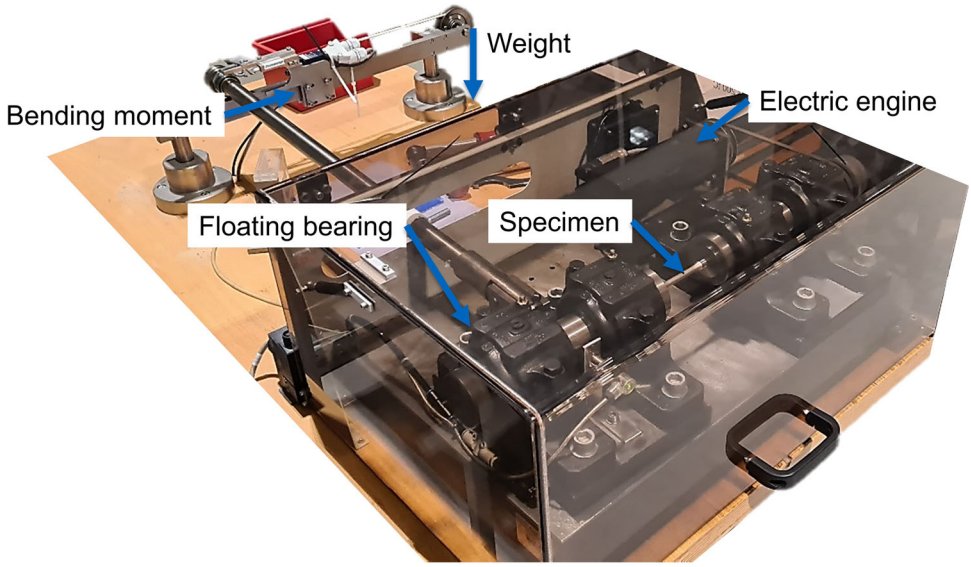

Fig. 3 Rotating bending test setup

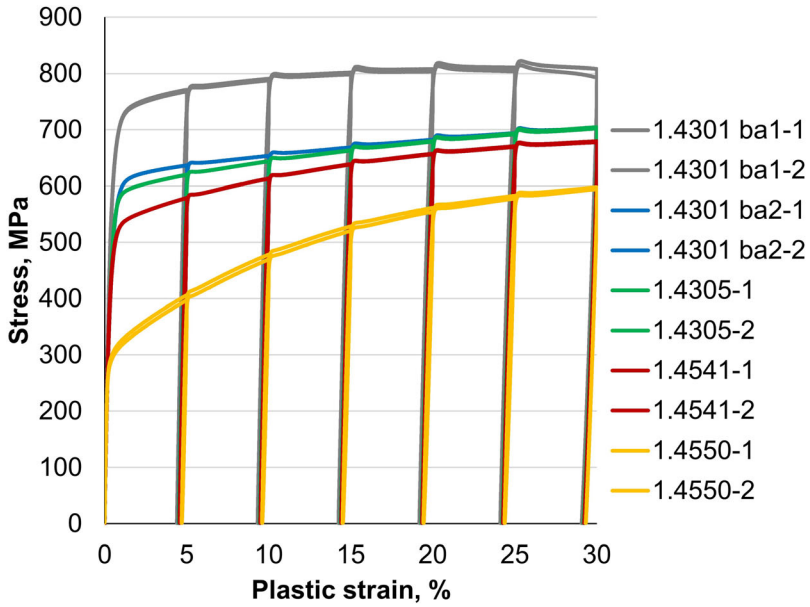

Material	σ_y, MPa
1.4301 batch1	620
1.4301 batch2	510
1.4305	500
1.4541	460
1.4550	300

Fig. 4 Stress strain diagram and 0.2 pct offset yield strength σ_y for each material tested; ba1 and ba2 refer to different batches

show similar plastic deformations and no necking had occurred. The influence of the specimen volume on the electromagnetic signal was nevertheless investigated. Analogous to the results from [28], a linear relationship between the test volume and the electromagnetic signals was observed.

As can be seen in Fig. 5, significant changes in signal can be detected at a testing frequency of 400 Hz with respect to the amplitude of the 1st harmonic 3rd harmonic as a function of plastic strain compared to the initial voltage.

Basically, two material behaviors can be observed in Fig. 5(a), the 1.4301 batch1 and 1.4541 show only a small amplitude increase with increasing strain. Furthermore, it can be observed that these materials have the largest starting amplitudes in the initial state. In contrast, the 1.4301 batch2, the 1.4305 and the 1.4550 show significant amplitude increases, whereby the incubation phase up to a significant amplitude increase varies depending on the plastic strain, see Fig. 5(c). The incubation phase from which martensite formation occurs is shown in Fig. 5(c) using the in-situ recorded measurement signal. An increase in amplitude can be seen for the 1.4301 batch2 from approximately 1.5% plastic strain. For 1.4305 and 1.4550, however, the amplitude increase begins at about 5% plastic deformation, and thus much later. In addition, small loops can be seen in 5% increments due to loading and unloading. The magnetic volume and magnetic properties can also be estimated from these loops, as these parameters also increase with greater loop formation. After approx. 30% plastic strain, the 1.4301 batch2 exhibits the highest 1st harmonic amplitude in total. In terms of the change compared to the starting amplitude, the 1.4550 shows an increase by a factor of 40.6. The 1.4301 batch2 shows an increase by a factor of 36.8.

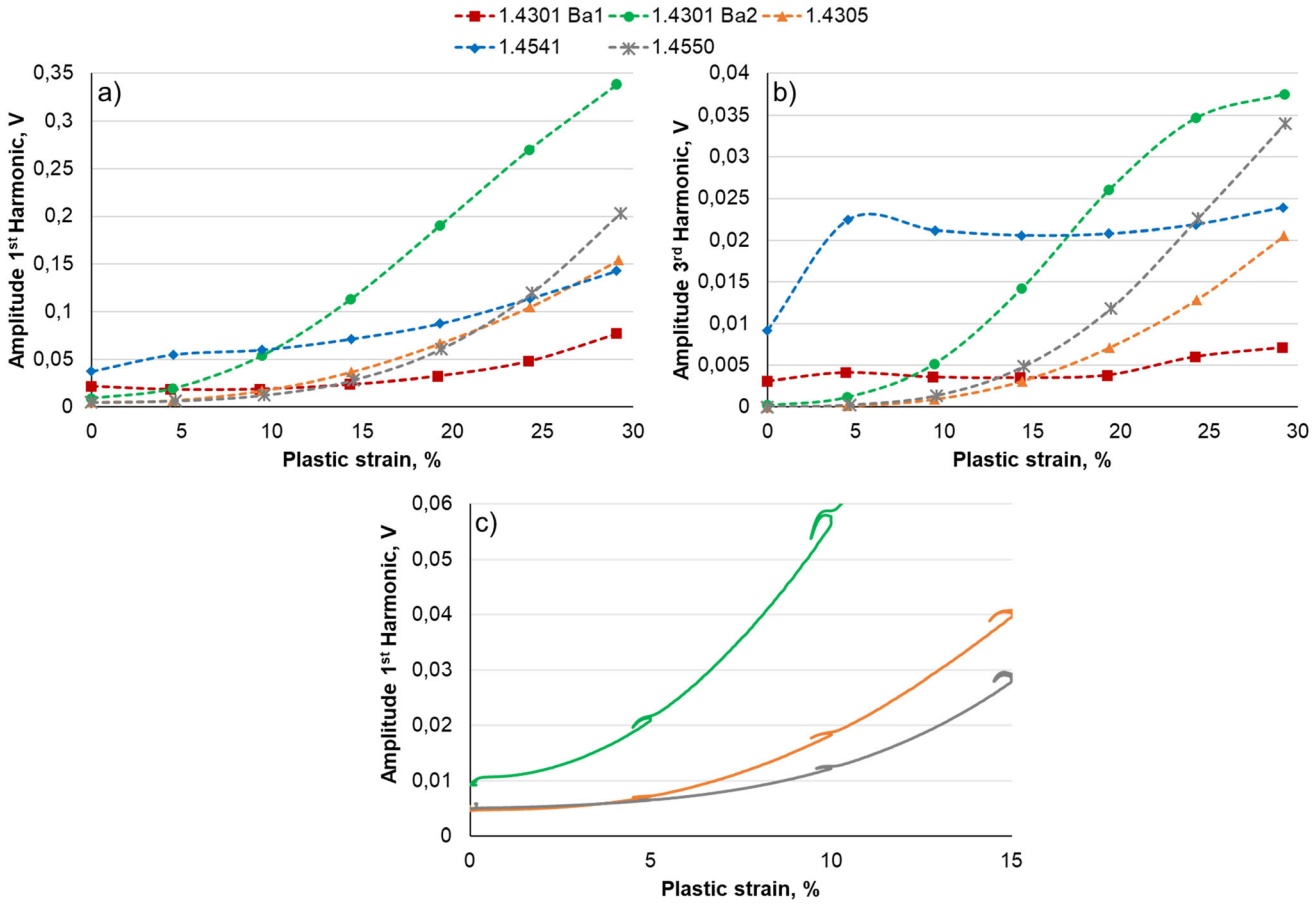

Fig. 5 Change of the amplitude in the unloaded state of (a) the 1st harmonic and (b) the 3rd harmonic as well as changes in the in-situ measurement signal in the 1st harmonic as a function of the plastic strain in (c)

As described in chapter 3.2, the 3rd harmonic is a value which indicates on the basis of the magnetic hysteresis curve whether ferromagnetic properties are present in the probed volume. In addition, from an increasing 3rd harmonic, higher magnetic permeabilities and thus also a higher proportion of martensitic phase can be inferred. With regard to the amplitude of the 3rd harmonic in Fig. 5(b), the materials 1.4301 batch1 and 1.4541 have a high starting amplitude, which indicates the presence of a magnetic phase. In the case of the 1.4305 and 1.4550, an amplitude was detected which corresponds to the noise of the measuring chain, while the 1.4301 batch2 is slightly above the noise limit. With increasing deformation, the amplitude of the 3rd harmonic increases exponentially for the materials 1.4301 batch2, 1.4305 and 1.4550 after different incubation phases, while the 1.4301 batch2 exhibits the highest increase at low plastic strains and after 20% deformation a significant decrease in the amplitude gradient. In direct comparison, no significant increase in amplitude is found for the 1.4301 batch1. The 1.4541, on the other hand, shows a significant increase in amplitude up to about 5% plastic deformation, with a small decrease thereafter followed by a small increase in amplitude.

For the in-situ test using a PCB sensor during the tensile tests, the eddy current signal was calibrated at the initial state. Accordingly, the test results give an operating point in the impedance plane which starts at the coordinate origin and changes in the impedance plane when there is a change in the electrical conductivity and/or the magnetic permeability in the probed volume. Figure 6(a) shows the change in amplitude of the eddy current signals as a function of plastic strain in the unloaded state, while Fig. 6(b) provides a closer look at the signal changes at low plastic strains.

The eddy current test was carried out at a frequency of 30 kHz. Within these tests, the 1.4550 and subsequently the 1.4301 batch2 showed the largest amplitude change. In this case as well, an increase in the amplitude can be used to infer the formation of martensite. The order with regard to the maximum amplitude change compared to the initial condition is identical to the order when considering the percentage amplitude change of the 1st harmonic. As can be seen from Fig. 6(b), the 1.4301 batch2 shows the greatest increase in amplitude, especially at the smaller plastic deformations. It should also be noted that the characteristic curve of the 1.4301 batch2 with a decrease in the amplitude gradient from about 20% deformation can also be seen, similar to the 3rd harmonic.

Nevertheless, with regard to the detection of overloads in the subsequent application, the chemical composition and microstructure of the 1.4301 batch2 is preferable to all other materials investigated, as it exhibits an early amplitude increase with the start of deformation in both electromagnetic test methods. After 4.5% plastic strain, an amplitude increase of 114% was registered for the 1st harmonic and 9 scale units for the eddy current test. Equivalently, smaller plastic strains can also be clearly differentiated. These results indicate that eddy current testing with a PCB sensor has the potential to detect minor structural changes.

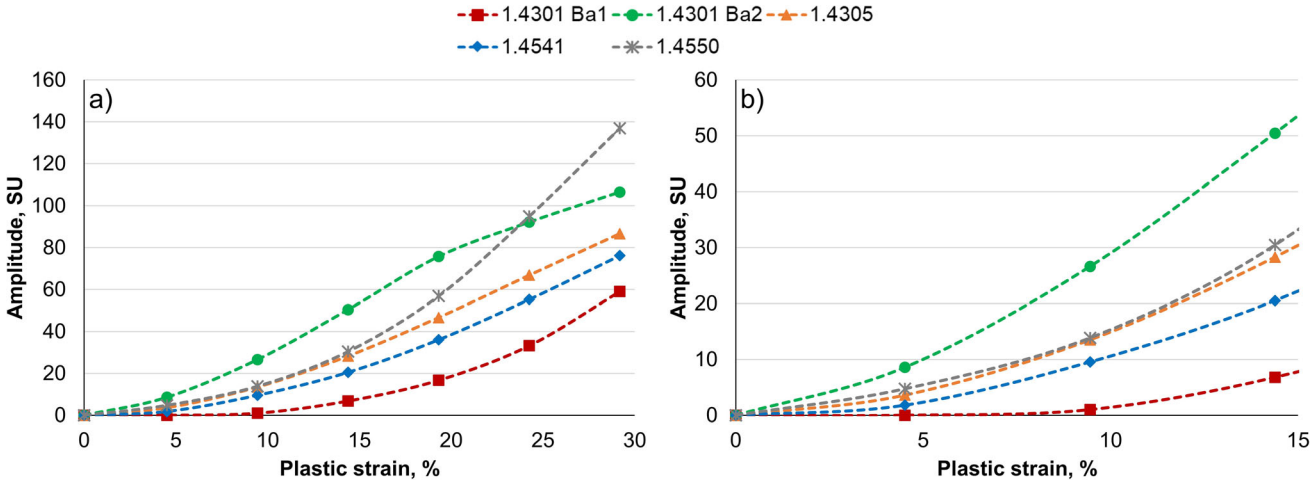

Fig. 6 (a) Change of the amplitude of the eddy current signals as a function of the plastic strain, (b) change of the amplitude with focus on low plastic strains

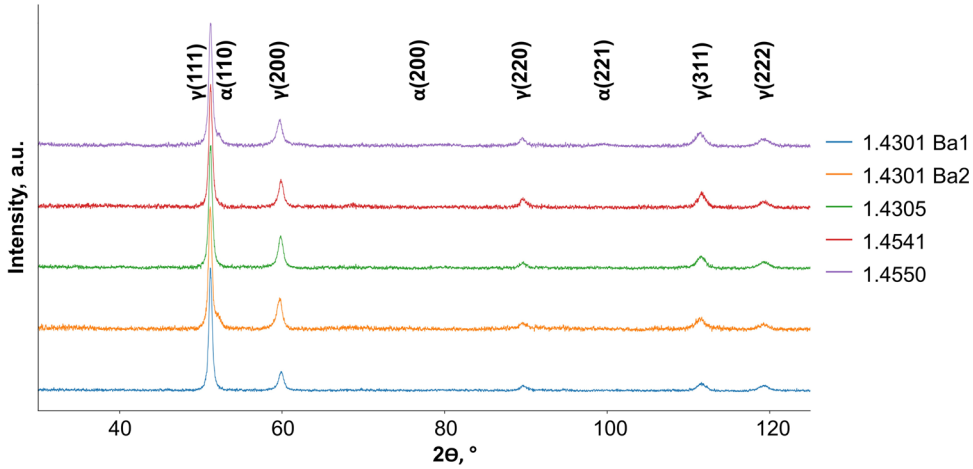

Fig. 7 XRD diffractograms of the initial state of the tensile specimens

Furthermore, the batch influence should be mentioned for 1.4301, as batch1 has a high austenite stability and batch2 a low austenite stability. In a direct comparison between the two batches (see Table 1), the nitrogen content in particular shows a clear difference. Batch2 has only one third of the nitrogen content of batch1. For the use as a material sensor, the selection of just an alloy is obviously not sufficient. This is also in agreement with the results of, e.g., [2, 4] and with the significant influence of the chemical composition on the metastability described in chapter 2.4.

For the validation of the electromagnetic test results with respect to the microstructural changes, XRD measurements were performed directly on the tensile specimen in the initial state and after 29% plastic strain. The measurement spot of approx. 0.5 mm was positioned in the center of the tensile specimen in each case. The results from the initial condition are shown in Fig. 7 including the γ- and α-phases.

As shown in Fig. 7, no martensitic phases were detected in the XRD measurements for the materials 1.4301 batch1, 1.4305 and 1.4541 in the initial state. The 1.4301 batch2 as well as 1.4550, on the other hand, show low intensity for the main (110) martensite reflex. However, the absence of a reflex does not necessarily mean that 0% martensite is present. According to [13], on the basis of quasi-static and cyclic tensile tests on the materials 1.4541 and 1.4550, a reliable determination of the fatigue state from about 10% martensite is possible with the aid of hardness tests and XRD measurements. In contrast, with the SQUID method, Feritscope measurements or conventional eddy current testing, a reliable determination of the fatigue state from 1% martensite is possible. In [30], different martensite contents of 1.4318 (AISI 301LN) and 1.4301 sheets were determined by Feritscope, Satmagan measurement, magnetic balance measurement, X-ray diffraction, density measurement and quantitative optical metallography and subsequently compared. XRD measurements showed strong differences due to the varying microstructure texture. Quantitative optical metallography turned out to be very time-consuming and inaccurate. The other methods yielded similar results.

The XRD results of the tensile specimens after a plastic deformation of 29% depending on the material are compared in Fig. 8. Clearly, there is a lower signal-to-noise ratio when compared to the data shown in Fig. 7. This is an effect of the increase in dislocation density and microstructural refinement upon plastic deformation.

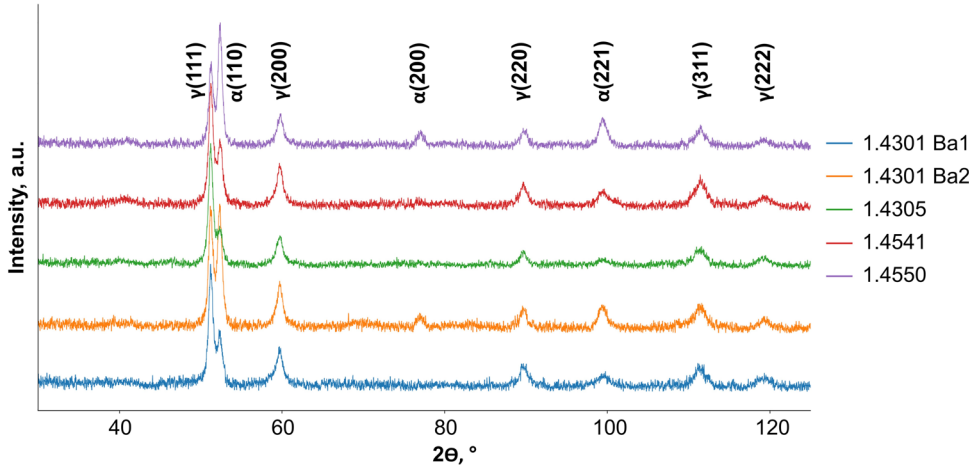

Fig. 8 XRD diffractograms after 29% elongation of the tensile specimens

The materials 1.4301 batch1, 1.4305 and 1.4541 show substantial martensite phase fractions, although the austenite content still clearly dominates after deformation. In contrast, the tensile specimen of 1.4301 batch2 shows reflexes, especially in the 111 and 110 planes, indicating similar contents of martensitic and austenitic phases. The tensile specimen from 1.4550 shows in total a larger content of the martensitic phase after an elongation of 30%. For the 1.4301 batch2 and the 1.4550, in addition to the reflexes from the main (110) martensite plane, reflexes are also observed in the (200) and (221) planes, indicating differences in texture formation.

By qualitatively considering the amplitude changes of the electromagnetic test signals with the phase contents from the XRD measurements after a plastic deformation of 29%, especially the 1.4301 batch2 as well as the 1.4550 appear promising with regard to the microstructural change. These two materials consequently exhibit the lowest austenite stabilities when plastic deformation sets in. Consequently, the most martensite was formed in these two alloys in comparison, which also results in a higher strength due to the mixed microstructure.

4.2 Rotating Bending Tests

Figure 9 presents selected test results from magnetic inductive measurements with harmonic analysis at a test frequency of 400 Hz. The microstructural changes in the rotating bending specimens were evaluated ex-situ without loading, and thus without the influence of the Villari effect. The last test before fatigue failure is indicated by the red symbol in Fig. 9.

Based on these data, the selected bending stresses and respective number of cycles to failure are:

- 1.4301 batch1: 434 and 496 MPa corresponding to 70 and 80% of the yield strength

– Fracture at 496 MPa after approx. 117,000 cycles

- 1.4301 batch2: 306, 357 and 383 MPa corresponding to 60, 70 and 75% of the yield strength

– Fracture at 357 MPa after approx. 330,000 cycles
– Fracture at 383 MPa after approx. 160,000 cycles

- 1.4305: 350 and 400 MPa corresponding to 70 and 80% of the yield strength

– Fracture at 400 MPa after approx. 267,000 cycles

- 1.4541: 250, 350, 368, 380 MPa corresponding to 55, 75, 80 and approx. 85% of the yield strength

– Fracture at 380 MPa after approx. 91,000 cycles

- 1.4550: 240, 270, 285 and 315 MPa corresponding to 80, 90, 95 and 105% of the yield strength

If 500,000 cycles were reached in the test, the bending stress was then increased in 5-10% steps. Due to the limited number of specimens per material, it should be noted that in most cases only one specimen could be fatigued per bending stress. Nevertheless, the respective material response to the different stresses could be derived from the test results. For all materials, it was observed that at a low bending stress, there was no significant increase in the amplitude of the 1st harmonic over the 500,000 cycles. An example were no relevant amplitude changes occurred is 1.4301 batch2 at a bending stress of 306 MPa.

From a stress threshold that is different for each material, an initial hardening takes place according to the selected stress. This initial hardening can be seen by a simultaneous increase in the amplitude of the 1st harmonic, e.g., slightly for the 1.4301 batch2 at a stress of 306 MPa and for the 1.4541 at all stresses up to a number of cycles of 50,000. If the initial hardening was not pronounced, an incubation phase followed by a steady microstructural change was observed, for example, in the curves of the 1.4541 at 368 MPa and the 1.4550 at 285 MPa. If the bending stress was increased further, the amplitude increased from the onset of the test. At the same time, it was observed that as the bending stress increases, the gradient of the amplitude change increases. Thus, with a known number of cycles, it could be possible to classify the previous load spectrum based on the difference in amplitude between two measurements. This can be seen in particular in the 1.4301 batch2, the 1.4541 and the 1.4550 from the 3-4 different amplitude curves. The 1.4550 shows a significant amplitude increase of 93% after 500,000 cycles at 315 MPa. At 330 MPa,

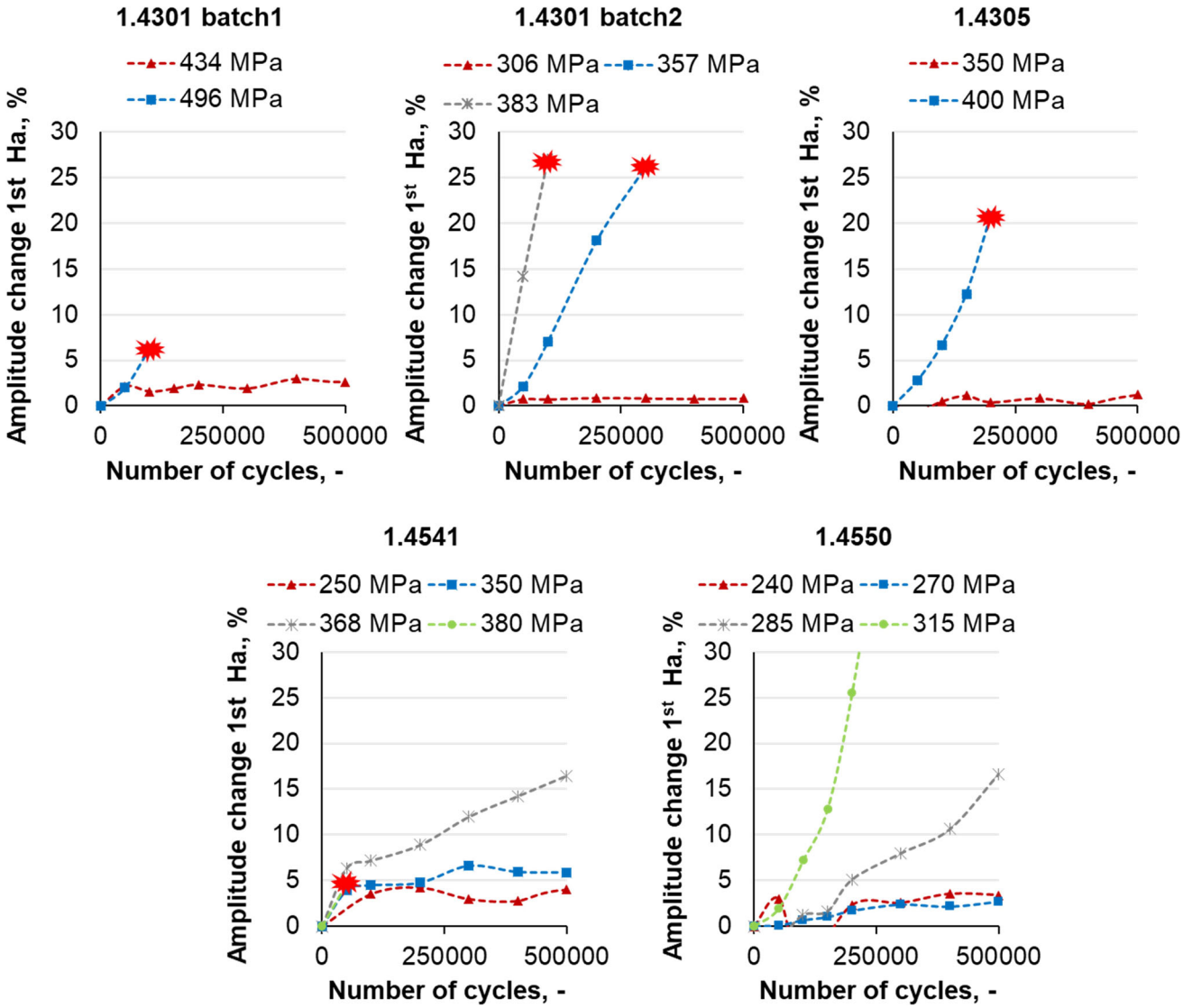

Fig. 9 Change in 1st harmonic amplitude as a function of bending stress and number of cycles for the different materials evaluated

however, the 1.4550 specimen broke after approx. 40,000 cycles, which means that no ex-situ test could be performed. From the curves of the 1.4301 batch2 and the similarly high amplitude change up to fracture of approx. 27%, it is evident that the amplitude change is dependent on both the load amplitude and the number of cycles, and thus on the accumulated applied deformation energy, but also on any temperature increases that occur at high bending stresses. In addition, the difference between the number of cycles of the last measurement and the number of cycles to fatigue failure must be taken into account when comparing the amplitude change, as significant signal changes can occur just before failure.

If an excessively high loading amplitude is selected for the material, fracture occurs within comparatively low numbers of cycles, although the amplitude of the 1st harmonic shows only slight changes. An exemplary curve with 6.7% amplitude change can be observed for the 1.4301 batch1 at a bending stress of 496 MPa. In the case of the 1.4541, on the other hand, the bending stress was increased to 380 MPa, resulting in a fracture after 91,000 cycles and an amplitude increase at 50,000 cycles of only 4.7%. In the case of the 1.4305, however, a 20% change in amplitude at 400 MPa was detected after 200,000 cycles before fatigue failure. It should be noted in this context that the change could be more pronounced shortly before fracture, but can only be detected with in-situ testing. A possible explanation for the small amplitude change of the 1.4301 batch1 and 1.4541 could be the temperature increase of the specimen during the rotating bending test, which increases with the bending stress and the number of cycles. At higher specimen temperature, less driving force for phase transformation is present. There is an indication of this for the 1.4541, as it already shows significant changes in the amplitude at a bending stress that is 12 MPa lower than the highest bending stress of 380 MPa. Temperature measurements during the tests were not performed. However, the influence of temperature on martensite formation was clearly demonstrated in [2, 14-16]. Furthermore, none of the fatigued specimens showed a tempering color on the fracture surface, which is characteristic for stainless steel due to the oxide layer formation as a function of the temperature.

The different transformation behavior of the alloys gives a first indication of their potential as material sensors. It is important that the material exhibits a large difference between the bending stress at which a relevant change can be detected and the stress at which fatigue failure occurs.

Following fatigue fracture or reaching 500,000 cycles, XRD measurements were also performed. The specimens that exhibited fatigue strength did not show martensite reflexes. As discussed in chapter 4.1, the detection of solely austenite reflexes does not mean that 0% martensite is present [13, 30]. In particular, stress-induced martensite formation is to be expected at the loads close to the fatigue strength. In [14], a martensite content of approx. 3% was determined for 1.4541 using eddy current testing technology after moderate stresses leading to 2 million cycles. Moreover, in [4], a magnetic indication of 4% for 1.4301 was measured by means of a Feritscope during tensile-compression tests in the LCF range.

An overload of the rotating bending specimens could be detected for the materials 1.4301 batch2, 1.4305, 1.4541 and 1.4550 on the basis of the amplitude change. Additionally, the material 1.4301 batch1 also exhibit an amplitude change until fracture, which, however, is smaller and also only occurred at loads that lead to fatigue fracture, and thus to strain-induced martensite formation. With regard to the estimation of austenite stability on the basis of M_{d30}, M_S and γ_{SF}, the 1.4301 batch2 and 1.4541 should have shown the greatest change in microstructure, followed in order by the 1.4550. In the investigations, however, the 1.4541 had a significantly greater austenite stability than the 1.4301 batch2 and the 1.4550. In comparison, the two batches of 1.4301 have a lower stacking fault energy, due to the low carbon and the high nitrogen content. In particular, the nitrogen content accounts for the largest difference between the two batches, whereby the content of the 1st batch is at the maximum allowable upper limit of the material. Furthermore, this is also the reason for the low M_{d30} and M_S temperatures. At the same time, this demonstrates the significant batch influence, as the difference between these batches is larger than to the other alloys. In summary, 1.4541 theoretically exhibits a low austenite stability, because in comparison it has the lowest Cr, Cu and N contents as well as a low C content. Thus, using the 3 parameters, a first indication of the metastability, e.g., for the 1.4301 batch2, can be obtained, but for the actual selection of the material, experiments have to be carried out.

With statistically validated amplitude curves and smaller steps between the selected bending stresses, and taking into account the ambient and specimen temperature, a material-specific critical threshold can be derived for the signal change. If the critical threshold is exceeded, it can be assumed that the structural integrity of the component is affected. With regard to the material behavior and the maximum amplitude change, the materials 1.4301 batch2 and 1.4550 or rather their chemical composition should also be preferred for cyclic loading.

One aspect that needs to be investigated further is the sequence of different loading amplitudes, as already pointed out in [2]. If pre-strengthening occurs during typical loading or a slightly higher non-critical loading, the subsequent microstructural change at a higher critical loading amplitude is less pronounced, leading to an underestimation of the fatigue state. In addition, it is of interest which possible microstructural changes, such as dislocation annihilation, occur in response to overloading in the subsequent typical loading condition.

In addition, an electromagnetic in-situ testing for the detection of microstructural changes is needed to collect high-quality information on the material behavior directly during the overloads. In the case of the test data from the specimens that exhibited fatigue failure below 500,000 cycles, only a snapshot is possible in each case due to the defined cycle numbers. This means that there may be significant amplitude increases in the subsequent cycles, but these cannot be seen in Fig. 9. As a result of crack initiation, strain-induced martensite formation also occurs, whereby a significant amplitude change can be expected within a few additional cycles. Nevertheless, an overload could be detected with a periodic inspection, e.g., every 50,000 cycles, although the intervals should not be too long to avoid missing critical events. An exemplary limit at which critical damage occurs could be an amplitude increase of 5%, taking into account the results from Fig. 9.

5. Conclusions

In order to find a suitable metastability for a material sensor that exhibits structural changes early before fatigue fracture, quasi-static tensile tests and cyclic rotating bending tests were carried out with the austenitic stainless steels 1.4301 batch1 and batch2 as well as the 1.4305, 1.4541 and 1.4550. For the detection of microstructural changes, magnetic inductive testing with analysis of higher-harmonic signal components and conventional eddy current testing were used in-situ in the tensile test and ex-situ in the rotating bending test after defined numbers of cycles. The following conclusions can be drawn:

- The materials 1.4301 batch2 and 1.4550 showed the highest electromagnetic signal change, and thus also the lowest austenite stability both in the tensile test and under cyclic bending stress. Due to the better mechanical properties, 1.4301 batch2 should be preferred.
- The order of the austenitic stainless steels tested was similar in terms of transformation behavior in both tests. Thus, the tensile test combined with in-situ electromagnetic testing appears to have potential as a suitable benchmark test for austenite stability. Regarding the estimation of austenite stability based on calculated values of M_{d30}, M_S and γ_{SF}, it was shown that comparative benchmark tests are necessary to validate these parameters.
- The microstructural changes in the tensile tests could be validated with the aid of XRD measurements. In contrast to the changes in the electromagnetic signal from the rotating bending tests, no martensite was detected by XRD. This indicates a low level of martensite formation, particularly at stress amplitudes close to fatigue strength.
- With regard to the cyclic bending stress, an overload of the specimens could be detected for the materials 1.4301 batch2, 1.4305, 1.4541 and for the 1.4550 on the basis of a significant amplitude change. At low bending stresses, uncritical for structural integrity, no increase in amplitude was measured.
- Unless the austenite stability of the alloy is too high, a periodic inspection, e.g., in the case of the rotating bending tests every 50,000 cycles, can be used to assess the fatigue state based on the amplitude of the electromagnetic test. If no increase of amplitude is measured, no critical overload has occurred. If, on the other hand, a critical

overload has occurred, an increase in amplitude due to martensite formation is measured. The maximum acceptable increase of amplitude must be determined on the basis of practical tests.

- It has been observed that as the bending stress increases, the gradient of the change in amplitude over the number of cycles increases as well. Thus, with a known number of cycles, it could be possible to classify the previous load spectrum based on the difference in amplitude between two measurements. However, further tests must follow, e.g., to include the influence of the load sequence.
- For the production of material sensors, the chemical composition must be accurately controlled. For instance, a high austenite stability was observed for the 1.4301 batch1, whereas the lower nitrogen content of batch 2 resulted in substantially different material response.

Funding

Open Access funding enabled and organized by Projekt DEAL. This study was funded by the Deutsche Forschungsgemeinschaft (DFG, German Research Foundation)—Project number 466760574 with the title ''Load sensitive spline shaft with sensory material''. The project is part of the SPP 2305 with the project number 441853410. The authors thank the DFG for financial support.

Conflict of interest

The authors declare no conflict of interest.

Open Access

References

1. R. Gansel, S. Zwoch, C. Heinrich, A. Lohrengel, H.J. Maier, and S. Barton, Identification of Overloads on Splined Shafts by Means of Eddy Current Testing Technology, Papers of the ECNDT 2023, *Res. Rev. J. Nondestruct. Test.*, 2023, **1**(1), p 1-6. https://doi.org/10.58286/28069
2. V. Schoß, Martensitische Umwandlung und Ermüdung austenitischer Edelstähle, Gefügeveränderungen und Möglichkeiten der Früherkennung von Ermüdungsschädigungen, Dissertation, Freiberg, Germany (2001)
3. C.P. Bemont, Trip steels as smart sensor alloys, Dissertation, KwaZulu-Natal, South Africa (2013)
4. M. Smaga, A. Boemke, T. Daniel, and M.W. Klein, Metastability and Fatigue Behavior of Austenitic Stainless Steels, *MATEC Web Conf.*, 2018, **165**, p 4010. https://doi.org/10.1051/matecconf/201816504010
5. G.B. Olson and M. Cohen, A Mechanism for the Strain-Induced Nucleation of Martensitic Transformations, *J. Less Common Met.*, 1972, **28**(1), p 107-118. https://doi.org/10.1016/0022-5088(72)90173-7
6. T. Angel, Formation of Martensite in Austenitic Stainless Steels Effects of Deformation, Temperature, and Composition, *J. Iron Steel Inst.*, 1954, **177**, p 165-174.
7. A.H. Bott, F.B. Pickering, and G.J. Butterworth, Development of High Manganese High Nitrogen Low Activation Austenitic Stainless Steels, *J. Nucl. Mater.*, 1986, **141-143**, p 1088-1096. https://doi.org/10.1016/0022-3115(86)90147-9
8. F.B. Pickering, Physical Metallurgical Development of Stainless Steels, *Conf. Proc. Stainl. Steels Goteborg*, 1984, **84**, p 1-281.
9. F. Lecroisey and A. Pineau, Martensitic Transformations Induced by Plastic Deformation in the Fe-Ni-Cr-C System, *Metall. Mater. Trans. B*, 1972, **3**(2), p 391-400. https://doi.org/10.1007/BF02642042
10. G.B. Olson and M. Cohen, Kinetics of Strain-Induced Martensitic Nucleation, *Metall. Mater. Trans. A*, 1975, **6**(4), p 791-795. https://doi.org/10.1007/BF02672301
11. S. Martin, O. Fabrichnaya, and D. Rafaja, Prediction of the Local Deformation Mechanisms in Metastable Austenitic Steels from the Local Concentration of the Main Alloying Elements, *Mater. Lett.*, 2015, **159**, p 484-488. https://doi.org/10.1016/j.matlet.2015.06.087
12. H. Schumann, Verformungsinduzierte Martensitbildung in metastabilen austenitischen Stählen, *Krist. Tech.*, 1975, **10**(4), p 401-411. https://doi.org/10.1002/crat.19750100409
13. F. de Backer, V. Schoss, and G. Maussner, Investigations on the Evaluation of the Residual Fatigue Life-Time in Austenitic Stainless Steels, *Nucl. Eng. Des.*, 2001, **206**(2-3), p 201-219. https://doi.org/10.1016/S0029-5493(00)00435-0
14. H.-J. Bassler, D. Eifler, M. Lang, and G. Dobmann, Characterization of the Fatigue Behavior of Austenitic Steel Using HTSL-SQUID, *Rev. Prog. Quant. Nondestruct. Eval.*, 1998 https://doi.org/10.1007/978-1-4615-5339-7_207
15. I. Nikitin and M. Besel, Effect of Low-Frequency on Fatigue Behaviour of Austenitic Steel AISI 304 at Room Temperature and 25°C, *Int. J. Fatigue*, 2008, **30**(10-11), p 2044-2049. https://doi.org/10.1016/j.ijfatigue.2008.02.005
16. M. Isakov, Strain Rate History Effects in a Metastable Austenitic Stainless Steel, Dissertation, Tampere, Finland (2012)
17. P. Hedström, L.E. Lindgren, J. Almer, U. Lienert, J. Bernier, M. Terner, and M. Odén, Load Partitioning and Strain-Induced Martensite Formation during Tensile Loading of a Metastable Austenitic Stainless Steel, *Metall. Mater. Trans. A*, 2009, **40**(5), p 1039-1048. https://doi.org/10.1007/s11661-009-9807-3
18. J. Talonen, H. Hänninen, P. Nenonen, and G. Pape, Effect of Strain Rate on the Strain-Induced $\gamma \rightarrow \alpha'$-Martensite Transformation and Mechanical Properties of Austenitic Stainless Steels, *Metall. Mater. Trans. A*, 2005, **36**(2), p 421-432. https://doi.org/10.1007/s11661-005-0313-y
19. B. Cao, T. Iwamoto, and P.P. Bhattacharjee, An Experimental Study on Strain-Induced Martensitic Transformation Behavior in SUS304 Austenitic Stainless Steel During Higher Strain Rate Deformation by Continuous Evaluation of Relative Magnetic Permeability, *Mater. Sci. Eng. A*, 2020, **774**, 138927. https://doi.org/10.1016/j.msea.2020.138927
20. S. Ganesh Sundara Raman and K.A. Padmanabhan, Influence of Martensite Formation and Grain Size on Room Temperature Low Cycle Fatigue Behaviour of AISI 304LN austenitic Stainless Steel, *Mater. Sci. Technol.*, 1994, **10**(7), p 614-620. https://doi.org/10.1179/mst.1994.10.7.614
21. A. Böhner, T. Niendorf, D. Amberger, H.W. Höppel, M. Göken, and H.J. Maier, Martensitic Transformation in Ultrafine-Grained Stainless Steel AISI 304L Under Monotonic and Cyclic Loading, *Metals*, 2012, **2**(1), p 56-64. https://doi.org/10.3390/met2010056
22. M. Oka, Y. Tsuchida, S. Nagato, T. Yakushiji, M. Enokizono, D.O. Thompson, and D.E. Chimenti, Estimation of Fatigue Damage for an Austenitic Stainless Steel (SUS304) Using a Pancake Type Coil, *AIP Conf. Proc.*, 2008, **975**(1), p 1244-1251. https://doi.org/10.1063/1.2902576
23. L.D. Thompson, B.D. Westermo, D.B. Crum, W. Law, R. Trombi, and R. Waldbusser, Smart structural fasteners for the aircraft and

construction industries, in *Proc. SPIE 3668, Smart Structures and Materials 1999: Smart Structures and Integrated Systems* 1999, p 143-152. https://doi.org/10.1117/12.350695
24. J.-M.V. Vugampore, Development of high strength material for smart aircraft bolt, Dissertation, KwaZulu-Natal, South Africa (2005)
25. K. Kinoshita, Inherent Magnetic Sensor for Estimation of Fatigue Damage in Type 304 Stainless Steel, *J. Nondestruct. Eval. Diagn. Progn. Eng. Syst.*, 2023, **6**, p 1. https://doi.org/10.1115/1.4054892
26. J.S. Dunning and L.D. Thompson, Development of Smart Solid State Structural Damage Assessment Systems for Underground Facilities, *Proc. Vol. 2447 Smart Struct. Mater. Ind. Commer. Appl. Smart Struct. Technol.*, 1995, **1995**, p 167-178. https://doi.org/10.1117/12.209330
27. B. Cao and T. Iwamoto, An Experimental Study on Strain Rate Sensitivity of Strain-induced Martensitic Transformation in SUS304 by Real-time Measurement of Relative Magnetic Permeability, *Steel Res. Int.*, 2017, **88**(12), p 1700022. https://doi.org/10.1002/srin.201700022
28. C. Celada-Casero, H. Kooiker, M. Groen, J. Post, and D. San-Martin, In-Situ Investigation of Strain-Induced Martensitic Transformation Kinetics in an Austenitic Stainless Steel by Inductive Measurements, *Metals*, 2017, **7**(7), p 271. https://doi.org/10.3390/met7070271
29. G. Mróz, W. Reimche, W. Frackowiak, O. Bruchwald, and H.J. Maier, Setting Discrete Yield-stress Sensors for Recording Early Component Loading Using Eddy-current Array Technology and Induction Thermography, *Procedia Technol.*, 2014, **15**, p 484-493. https://doi.org/10.1016/j.protcy.2014.09.008
30. J. Talonen, P. Aspegren, and H. Hänninen, Comparison of Different Methods for Measuring Strain Induced α-Martensite Content in Austenitic Steels, *Mater. Sci. Technol.*, 2004, **20**(12), p 1506-1512. https://doi.org/10.1179/026708304X4367
31. C.P. Bemont, The Development of Robust Structural Health Monitoring Sensors Utilizing TRIP Steel, *IEEE Sens. J.*, 2009, **9**(11), p 1449-1455. https://doi.org/10.1109/JSEN.2009.2021801
32. G. Mróz, Entwicklung von Techniken zur bauteilinhärenten Informationsspeicherung und Erfassung von Bauteilbelastungen, Dissertation, Hannover, Germany (2013)
33. B. Wielage, T. Mäder, D. Nestler, T. Schurig, B. Michaelis, and S. Sievers, Belastungsmonitoring an Faserverbundwerkstoffen unter Ausnutzung der Gefügeumwandlung von Sensordrähten. Load monitoring in fibre composites utilising the microstructural transformation of sensor wires, *Materialwiss. Werkstofftech.*, 2010, **41**(6), p 430-436. https://doi.org/10.1002/mawe.201000623
34. L.D. Thompson, B.D. Westermo, New strain measurement technology for material damage assessment, in *Proc. SPIE 2191, Smart Structures and Materials 1994: Smart Sensing, Processing, and Instrumentation*, p 380-391 (1994). https://doi.org/10.1117/12.173968
35. N. Bowler, Eddy-Current Nondestructive Evaluation, Springer eBooks Chemistry and Materials, *Science*, 2019 https://doi.org/10.1007/978-1-4939-9629-2
36. J. García-Martín, J. Gómez-Gil, and E. Vázquez-Sánchez, Non-destructive Techniques Based on Eddy Current Testing, *Sensors*, 2011, **11**(3), p 2525-2565. https://doi.org/10.3390/s110302525,28.02.2011
37. M. Bernard, C. Scheer, V. Böhm, and W. Reimche, New Developments in Non-destructive Testing for Quality Assurance in Component Manufacturing, *Steel Res. Int.*, 2009, **80**(12), p 916-928. https://doi.org/10.2374/SRI09SP144
38. L.V. Fricke, H.N. Nguyen, B. Breidenstein, D. Zaremba, and H.J. Maier, Eddy Current Detection of the Martensitic Transformation in AISI304 Induced upon Cryogenic Cutting, *Steel Res. Int.*, 2021, **92**(1), p 2000299. https://doi.org/10.1002/srin.202000299
39. O. Bruchwald, W. Frackowiak, W. Reimche, and H.J. Maier, Non-destructive In Situ Monitoring of the Microstructural Development in high Performance Steel Components During Heat Treatment, *La Metallurgia Italiana*, 2015, **11**(12), p 29-37.
40. S. Barton, W. Reimche, and H.J. Maier, Three-Dimensional Data Storage in the Subsurface Region and Fast Read-Out Technologies for Determining the Mechanical Load History of Components, *HTM J. Heat Treat. Mater.*, 2018, **73**(1), p 13-26. https://doi.org/10.3139/105.110343
41. I. Roth, Untersuchungen zum Ausbreitungsverhalten mikrostrukturell kurzer Ermüdungsrisse in metastabilem austenitischen Edelstahl, Dissertation, Siegen, Germany (2012)
42. C. Müller-Bollenhagen, M. Zimmermann, and H.-J. Christ, Very High Cycle Fatigue Behaviour of Austenitic Stainless Steel and the Effect of Strain-Induced Martensite, *Int. J. Fatigue*, 2010, **32**(6), p 936-942. https://doi.org/10.1016/j.ijfatigue.2009.05.007